Title

Multi-technique approach to study the stability of silver nanoparticles at predicted environmental concentrations in wastewater

Journal

Water Research, 166

ISSN

0043-1354

Authors

Cervantes-Avilés, Pabel

Huang, Yuxiong

Keller, Arturo A

Publication Date

2019-12-01

DOI

10.1016/j.watres.2019.115072

Peer reviewed

Water Research 166 (2019) 115072

Contents lists available at ScienceDirect

Water Research

journal homepage: www.elsevier.com/locate/watres

Multi-technique approach to study the stability of silver nanoparticles at predicted environmental concentrations in wastewater

Pabel Cervantes-Avilés [a, b], Yuxiong Huang [b, c], Arturo A. Keller [a, b, *]

[a] Bren School of Environmental Science and Management, University of California, Santa Barbara, CA, 93106, USA
[b] UC Center for Environmental Implications of Nanotechnology, University of California, Santa Barbara, CA, 93106, USA
[c] Shenzhen Environmental Science and New Energy Technology Engineering Laboratory, Tsinghua-Berkeley Shenzhen Institute, Shenzhen, 518055, PR China

ARTICLE INFO

Article history:
Received 23 May 2019
Received in revised form
4 September 2019
Accepted 7 September 2019
Available online 9 September 2019

Keywords:
Single particle ICP-MS
Nanoparticle tracking analysis
Surface plasmon resonance
Ag NP
Dissolution
Wastewater treatment plant

ABSTRACT

The concentration of silver nanoparticles (nano-Ag) in aqueous media influences the kinetics of ion release; hence, the transformation and stability of nano-Ag are also influenced. The stability, dissolution and further transformation of nano-Ag in aqueous media at predicted environmental concentrations (PECs) $\leq$ μg/L may differ from that reported at higher concentrations. Analytical techniques characterizing nanoparticles (NPs) at μg/L have advantages and limitations, including an inherent bias based on theoretical and analytical considerations, as well as the matrix effects. In this work, we applied nanoparticle tracking analysis (NTA), single particle ICP-MS (sp-ICP-MS), and localized surface plasmon resonance (LSPR) analysis to study the stability and dissolution of nano-Ag with different nominal sizes (20, 40, 80 and 100 nm) at PECs in synthetic wastewater (SWW). The influence of the main wastewater constituents, such as organic matter, Cl^-, S^{2-}, PO_4^{3-} and NH_4^+, on the stability and dissolution of nano-Ag (40 nm) at PECs was also determined. Diagrams of the predominant species of silver exposed to major ligands were generated using MINTEQ. After 5 h in SWW, 20 nm nano-Ag dissolved 19.27% and 40 nm nano-Ag dissolved 14.8%. Aggregates of Ag particles were clearly noted for 80 and 100 nm nano-Ag after 5 h of exposure to SWW. Aggregates size also ranged very similar for both techniques, NTA and sp-ICP-MS, 29–211 nm and 38–241 for NTA and 48–210 and 50–220 nm, for sp-ICP-MS, respectively. Monodispersed size distribution (22–85 nm) and low dissolution (up to 5.1%) of nano-Ag at PECs were observed in presence of organic matter (5–800 μg/L) and PO_4^{3-} (9.5–47.5 mg/L), while precipitation and higher dissolution (up to 74.9%) were observed in media containing either Cl^- (0.07–10.64 g/L), S^{2-} (0.32–32.1 mg/L) or NH_4^+ (36–90 mg/L), respectively. Speciation diagrams predict the formation of $Ag_2S_{(s)}$ and $AgCl_{(s)}$, and soluble species such as $AgCl_x^{(x-1)-}$, $AgNH_3^+$ and $Ag(NH_3)^{2+}$ when Ag^+ at PECs in wastewater. The NTA and sp-ICP-MS were suitable techniques for sizing nano-Ag in wastewater at PECs at experimented nominal sizes. sp-ICP-MS was also useful to quantify the coexistence of Ag^+ and nano-Ag. The LSPR analysis served to determine the relative persistence of original nano-Ag at PECs in the wastewater during the first 5 h after spiking.

1. Introduction

Silver nanoparticles (nano-Ag) are incorporated in products due to their known antibacterial activity (Zhang et al., 2018). Goods containing nano-Ag include water filters, paints, cosmetics, deodorants, clothing, textiles, food packaging, functionalized plastics, medical devices, wound dressings, among others (Cascio et al., 2015; McGillicuddy et al., 2017). The expected release of nano-Ag and silver ions (Ag^+) from these products has raised concerns about their potential effects with regard to health and the environment (Sekine et al., 2015; Westerhoff et al., 2018). The pathways for release of nano-Ag and other engineered nanomaterials (ENMs) in the environment have being studied via modeling (Keller and Lazareva, 2013; Lazareva and Keller, 2014; Sun et al., 2016) and via nanometrology (Lead et al., 2018). This last approach includes physical and chemical techniques to detect, quantify or characterize the ENMs in the environmental matrices (Bitragunta et al., 2017; Kaegi et al., 2013; Mitrano et al., 2012). In both approaches, models

* Corresponding author. Bren School of Environmental Science and Management, 3420 Bren Hall, University of California, Santa Barbara, CA, 93106, USA.
E-mail address: keller@bren.ucsb.edu (A.A. Keller).

https://doi.org/10.1016/j.watres.2019.115072
0043-1354/

and nanometrology, wastewater treatment plants (WWTPs) have been considered as a crucial barrier that can remove the NPs released to the wastewater before they enter the environment (Cao et al., 2018; Lazareva and Keller, 2014; Westerhoff et al., 2015). In many cases, WWTPs can remove over 90% of NPs, as the sewage passes throughout the physical, chemical and biological treatment processes (Cervantes-Avilés et al., 2019; Kaegi et al., 2013; Westerhoff et al., 2018). Some transformation of the ENMs, such as nano-Ag, is expected before, during and after wastewater treatment facilities: in the sewer, in the WWTP and later when the effluent is discharged into water bodies (Brunetti et al., 2015; Li et al., 2013; Ma et al., 2013). Therefore it is important to understand that the potential fate and health effects of the original NPs may not reflect those of the materials that are discharged into the environment (Zhang et al., 2016).

The main transformation processes of nano-Ag in environmental media have been studied widely (Kaegi et al., 2013; Levard et al., 2012; Yu et al., 2016; Zhang et al., 2018). However, most studies have considered NPs at mg/L levels to minimize errors (e.g. due to detection limits) in several techniques applied to study the stability, size, dissolution and transformation processes of NPs (e.g., dynamic light scattering (DLS), transmission electron microscopy (TEM), scanning electron microscopy (SEM), atomic force microscopy (AFM), fluorescence correlation spectroscopy (FCS), and field flow fractionation (FFF)). For example, a multimethod characterization at 1, 30 and 100 mg/L of ZnO and TiO_2 NPs in environmental media showed differential aggregate formation at the various concentrations, indicating that the number of particles influences their stability (Domingos et al., 2009). Since the predicted environmental concentrations (PECs) of many ENMs, including nano-Ag in aquatic environments, are at μg/L levels and below (Lazareva and Keller, 2014; Maurer-Jones et al., 2013), there is a need to understand the stability and transformation of these ENMs under more realistic conditions.

In addition to the NP concentration levels, NP size, conditions and characteristics of the media can influence ENM stability and dissolution rate (Ivask et al., 2014). The stability of nano-Ag in aquatic environments is influenced by temperature and pH (McGillicuddy et al., 2017), ultraviolet−visible radiation (Li et al., 2018; Yu et al., 2016), organic matter content (Delay et al., 2011; Lowry et al., 2012; Yu et al., 2016) and ionic strength (Delay et al., 2011; Li et al., 2018). The stability and dissolution of nano-Ag are also affected by particular ligands, such as Cl^- (Levard et al., 2013b; Li et al., 2018), S^{2-} (Kaegi et al., 2013; Levard et al., 2011, 2013a), and O_2^- (Zhang et al., 2018), which form stable species of silver such as AgCl, Ag_2S and Ag_2O, respectively (Lowry et al., 2012; Zhang et al., 2018). In wastewater, some of the soluble constituents can influence nano-Ag transformations (Doolette et al., 2013). For example, SO_4^{2-} can be anaerobically reduced to S^{2-} in the sewer, which may form Ag_2S when Ag^+ is present. The transformation of nano-Ag into Ag_2S in a sewer channel was studied by using extended X-ray absorption fine structure (EXAFS) techniques (Kaegi et al., 2013). Results showed the crystallization of Ag_2S and coarsening of an Ag_2S shell on the surface of the nano-Ag (Kaegi et al., 2013), making the NPs less toxic than the original nano-Ag (Levard et al., 2012, 2013a). However, sulfidization occurred at 3.8−4.8 mg/L of S^{2-} when 50 mg/L nano-Ag were spiked into a sewer channel (Kaegi et al., 2013). Although the S^{2-} concentrations were in the expected range for municipal wastewater (3−19 mg/L) (Metcalf and Eddy, 2014), the spiked Ag concentration were much higher than PECs = 2−18 μg/L (Blaser et al., 2008) and measured concentrations of nano-Ag in wastewater between 14 ng/L (Cervantes-Avilés et al., 2019) and 200 ng/L (Mitrano et al., 2012). Since the concentration of nano-Ag limits the kinetics of ion release (Zhang et al., 2018), the formation of Ag_2S in the presence of nano-Ag at the PECs may differ from studies at mg/L level.

The interaction between Cl^- and nano-Ag in water results in the precipitation of $AgCl_{(s)}$. This process has a strong dependence on Cl/Ag molar ratios, but the studies were performed at 2−215 mg/L of nano-Ag and 0.6−29 g/L of NaCl (Levard et al., 2013b); results at PECs may differ substantially since the Cl/Ag molar ratios will be quite different. The formation of an $AgCl_{(s)}$ shell was also reported when 0.2 mg/L nano-Ag was exposed to 0.6 g/L of NaCl (Li et al., 2018). The Cl^- concentrations expected in some aquatic environments such as wastewater, reclaimed water and surface water are 0.03−0.3 g/L (APHA, 2005), which are generally lower than those used in several transformation experiments (0.6−29 g/L) (Impellitteri et al., 2009; Levard et al., 2013b; Li et al., 2018). Since the stability and dissolution of nano-Ag for low Cl^- conditions remains poorly understood, studies at more realistic concentration scenarios of both Cl^- and nano-Ag are needed to determine the dissolution pattern of nano-Ag, the formation of $AgCl_x^{(x-1)-}$ species, and the size distribution of the persisting nano-Ag. In addition to the ligands mentioned above (S^{2-} and Cl^-), wastewater contains some other major chemical compounds, such as NH_4^+ and PO_4^{3-}, which can influence the stability, dissolution and later transformation of nano-Ag during their transport in the sewage.

The sources of municipal wastewater flow are residential areas, commercial districts, facilities for recreational activities, and educational institutions (Lusk et al., 2017; Metcalf and Eddy, 2014). The main constituents of municipal wastewater are organic and inorganic solids, soluble compounds such as organic matter, organic nitrogen (e.g. urea) and inorganic nitrogen (e.g., NH_4^+, NO_3^-, NO_2^-), organic and inorganic phosphorus (Cervantes-Avilés et al., 2017; van Loosdrecht et al., 2016), and other major ions such as SO_4^{2-}, CO_3^{2-}, Na^+ and Cl^-. The concentration of wastewater constituents vary according to several factors, including flowrate, population, and even the season (Jin et al., 2017; Liu et al., 2016). Information on the effects of the variability of these factors on the stability of nano-Ag at PEC is also scarce.

As stated earlier, the detection level of some measurement techniques has led to use NP concentrations much higher than PECs during characterization experiments. Nevertheless, the use of multiple analytical techniques when characterizing NPs has been strongly recommended to differentiate their inherent bias (Brar and Verma, 2011; Domingos et al., 2009; Louie et al., 2016), due to differences in preparation techniques and fundamental principles. Nanoparticle tracking analysis (NTA) (Carr and Wright, 2013; Mehrabi et al., 2017) and single-particle inductively couple plasma − mass spectrometry (sp-ICP-MS) (Degueldre and Favarger, 2003; Donovan et al., 2016; Laborda et al., 2014; Montaño et al., 2014) are techniques used for particle sizing with minimum sample preparation. NTA has multiple applications in nanomedicine, including the characterization of ENMs carrying drugs in complex systems (Carr and Wright, 2013), and the sizing of reference materials such as Au particles (Mehrabi et al., 2017; Roesslein, 2018). As with other sizing techniques, sedimentation of NPs may take place during the NTA at mg/L levels (Domingos et al., 2009). However, the advantages of NTA include a lower concentration detection limit compared to DLS, as well as the visualization and characterization of NPs at PECs (Korenstein et al., 2013). sp-ICP-MS is another technique that can be used to quantify and characterize NPs at ng/L (Cervantes-Avilés et al., 2019; Hadioui et al., 2014; Mitrano et al., 2012; Montaño et al., 2014), and determine the ionic concentration released from the NPs at PEC levels in environmental and complex matrices (Azimzada et al., 2017). The simultaneous use of sp-ICP-MS and NTA can yield new insights on the stability of NPs at PECs in complex media that was not possible to observe with previous methods due to their high detection limits.

Understanding the stability of nano-Ag at PECs, and their

transformation into soluble and insoluble Ag products under realistic water conditions is relevant for the detection and quantification of nano-Ag in real environmental media, ecotoxicological studies, life cycle risk assessments and their regulation. In this work, we determined the stability and dissolution of nano-Ag with different nominal sizes (20, 40, 80 and 100 nm) at realistic concentrations in wastewater by a multi-technique approach. We also studied the influence of the main ligands and other important constituents of wastewater on the stability and dissolution of nano-Ag. The multi-technique approach included the NTA, sp-ICP-MS, and the localized surface plasmon resonance (LSPR). Modeling of the chemical interactions between ligands and Ag^{+} was also carried out.

2. Materials and methods

2.1. Materials

Deionized (DI) water at constant 18.2 MΩ/cm was obtained from a NANOpure water purification system (Thermo Scientific), and used in all NPs suspensions and solutions. Synthetic wastewater (SWW) was prepared according to a previous study (Cervantes-Avilés et al., 2016). In brief, 380.4 mg/L D-Glucose (Sigma-Aldrich), 45.1 mg/L NH_4OH (14.8 M, Fisher Scientific), 14.4 mg/L K_2HPO_4 (Sigma-Aldrich), 14.2 mg/L NaCl (Sigma-Aldrich), 8.8 mg/L $MgSO_4 \cdot 7H_2O$ (Fisher Scientific) and 3.8 mg/L $CaCl_2 \cdot 2H_2O$ (Fisher Scientific) were mixed. NaCl, K_2HPO_4 and NH_4OH were also used in selected experiments. NaOH (Sigma-Aldrich) and HNO_3 (BDH Aristar® Ultra grade) were used to adjust pH at 7 of SWW and experiments. Na_2S (Fisher Scientific) was dehydrated at 105 °C for 24 h before use. Suwannee River natural organic matter (SRNOM) was obtained from the International Humic Substances Society and used as natural organic matter (NOM) source in selected experiments.

A 50 mg/L suspension of Au nanoparticles, with nominal size of 60 nm in 2 mM sodium citrate, was purchased from NanoComposix Inc., and used for calibration in the NTA studies and as reference material in sp-ICP-MS measurements. Stock aqueous suspensions (20 mg/L) of nano-Ag coated with polyvinylpyrrolidone (Ag-PVP), with nominal sizes of 20, 40, 80 and 100 nm, were purchased from Sigma-Aldrich. Ethanol (99.5%) ACS reagent absolute (ACROS Organics™) for cleaning of the LM10 viewing unit in the NTA.

Certified ionic standards of Au (100 μg/mL) and Ag (10 μg/mL) in 2% HCl and 2% HNO_3 (Agilent Technologies Inc), respectively, were used as the corresponding elemental response factor during sp-ICP-MS measurements. HCl (34–37%) and HNO_3 (67–70%) of ultra-high purity for quantitative trace metal analysis at the parts-per-trillion (ng/L) level (BDH Aristar® Ultra grade) were used to dilute the calibration ionic standards. Chelex-100 resin with 50–100 mesh and a capacity of 0.7 meq/mL was acquired from Sigma-Aldrich and used to remove the ionic form of silver immediately before sp-ICP-MS measurements. Polypropylene tubes with 1.6 mm of internal diameter and 14 cm of effective length were used as a column for the Chelex-100 resin. Glass wool (Sigma-Aldrich) was placed at the beginning and end of the columns. All solutions and suspensions were prepared in metal-free polypropylene tubes.

2.2. Ag nanoparticles characterization

The Ag-PVP NP suspensions (1 mg/L) in DI water of all the sizes were characterized in terms of the zeta potential (ZP), LSPR (UV 1800; Shimadzu) and size. Before analysis, Ag-PVP NP suspensions were sonicated for 20 min at 280 W and a frequency of 40 kHz by using an ultrasonic bath (Bransonic, Emerson). ZP was determined by Laser Doppler Velocimetry (Zetasizer Nano ZS90, Malvern Panalytical Ltd). LSPR was determined by the absorption spectra (300–600 nm) in the UV–vis Spectrophotometer (UV, 1800; Shimadzu), which was equipped with a halogen lamp. Size was determined via NTA (NanoSight LM10, Malvern Panalytical Ltd.). Ethanol (99.5%) was used to clean the LM10 viewing unit in between samples.

2.3. Nanoparticle tracking analysis (NTA)

NTA was used to determine the size distribution of Ag-PVP NPs in SWW and in the particular water constituents, such as NOM, Cl^{-}, S^{2-}, PO_4^{3-}, and NH_4^{+}. Measurements were performed in the NanoSight LM10, with a laser output of 65 mW at 405 nm. The NanoSight was equipped with a Scientific CMOS camera, which worked at 20X magnification during all experiments. Size calibration was performed using nano-Ag (40 nm) and Au NPs (60 nm) at 100 μg/L in DI water, which were measured during pre-processing of samples to optimize the parameters in terms of particle concentration and size. The operating parameters are reported in Table 1, and were according to the parameters validated by the European Nanomedicine Characterisation Laboratory (EUNCL) for NTA (Roesslein, 2018). Samples were measured five times with 30 s captures. Data collection and further analysis were conducted by using the NTA 2.3 Analytical Software. Around 2,000 frames were processed for each sample, with at least 6,000 tracks per run. The inlet and outlet ports of the LM10 cell were capped after uploading the samples. NTA studies were performed no more than 1 h after sample preparation. The results reflect the size distribution that occur 90% and 50% of the time, as well as the median size.

2.4. Single particle ICP-MS (sp-ICP-MS) analysis

The concentration of the nano-Ag and their size distribution after exposure to SWW and the different solutions (NOM, Cl^{-}, S^{2-}, PO_4^{3-} and NH_4^{+}) were determined using an Agilent 7900 ICP-MS (Santa Clara, CA, USA) with the sp-ICP-MS software module. The instrument was equipped with an auto sampler and a standard peristaltic pump, standard glass concentric nebulizer, quartz spray chamber and quartz torch, standard nickel sampling and skimmer cones. Analyses were performed in time-resolved analysis (TRA) mode using a dwell time of 100 μs per point without settling time between measurements, as previously reported (Keller et al., 2018; Montaño et al., 2014). The transport efficiencies for Au and Ag are almost identical; however, Au NPs are more stable than nano-Ag (Wimmer et al., 2018). Therefore, we used Au NPs (60 nm in diameter) in sodium citrate buffer (NanoComposix Inc.) diluted to 100 ng/L with DI water to evaluate the nebulization efficiency, which was used for data conversion from raw signal to NP size. The Ag ionic standard was diluted to 1 μg/L with 1% HNO_3 and was used to determine the elemental response factor. The instrument settings used for the sp-ICP-MS analysis are summarized in Table 2.

Table 1
NanoSight LM10 operating conditions used in experiments.

Parameter	Operation Setting
Camera level	9
Screen gain	0.94
Detection Threshold	10
Blur	3 × 3
Minimum track length	15 steps
Minimum expected particle size	30 nm, 17.9 pixels
Bin width	2 nm
Temperature	22 °C
Water viscosity	0.95 (10^{-3} kg/m·s)

Table 2
Agilent 7900 sp-ICP-MS operating conditions.

Parameter	Operation Setting
Reference material	100 ng/L Au NPs 60 nm
RF power	1550 W
Carrier gas flow	0.67 L/min
Sample inlet flow	0.346 mL/min
Nebulizer pump velocity	0.1 revolutions per sec
Acquisition time	90 s
Dwell time	100 μs
Mass monitored	^{107}Ag
Density of nAg	10.5 g/mL

The samples were diluted with DI water to ensure the nano-Ag concentrations were between 50 and 500 ng/L. To make sure that the samples were fully homogenized after dilution, they were vortexed at 5,000 rpm for 2 min. Then, the samples were passed throughout a Chelex-100 column to avoid false positives by ionic silver during sp-ICP-MS measurements (Azimzada et al., 2017; Hadioui et al., 2014). Before each sample, Chelex-100 column was regenerated by washing with 5 beds volumes of 1 N HCl, 5 bed volumes of DI water at pH 7, 5 bed volumes of 1 N NaOH, and 5 bed volumes of DI water at pH 7. The sp-ICP-MS method setup, data collection, and analysis were controlled via the Single Nanoparticle Application Module (method wizard) in the Agilent ICP-MS MassHunter software (Version C.01.03 Build 505.16 Patch 3), as in our previous study (Cervantes-Avilés et al., 2019). Results of nano-Ag correspond to the mean and standard deviation of triplicate measurements. Ag^+ form (i.e., dissolved Ag) was calculated from the difference between the initial Ag load of the samples and the nano-Ag concentration measured.

2.5. Stability of Ag-PVP NPs in synthetic wastewater (SWW) over time

The size distribution of Ag-PVP NPs and the dissolved Ag in SWW were evaluated at times 0 and 5 h for each nominal size of 20, 40, 80 and 100 nm. Two sets of tubes containing SWW were prepared for each nominal size. Tubes were spiked with 100 μg/L Ag-PVP NPs of their respective nominal size. All tubes were sonicated for 15 min. One set of tubes of each nominal size was left to stand for 5 h and the other was analyzed immediately. In both sets of tubes, Ag-PVP NPs were sized by both NTA and sp-ICP-MS analysis. Sedimentation was monitored during the 5 h by using the UV–vis spectrophotometer, which measured the absorbance at LSPR of the nanoparticles every min for 300 min (5 h) in SWW and in DI water as control. The experiments were performed in triplicate, and the results presented are the average of the runs.

2.6. Influence of NOM and Cl^- on the size and surface charge of Ag-PVP NPs

The effects of NOM (5–800 μg/L) and Cl^- (0.07–10.64 g/L) on 40 nm Ag-PVP NPs were evaluated by measuring ZP, size, as well as the dissolved Ag from Ag particles. Particle size distribution was measured via NTA. All experiments containing either NOM or Cl^- were spiked by the same concentration of Ag-PVP NPs (100 μg/L). Tubes were sonicated for 15 min, and left to stand 1 h. Then, samples were collected for size, ZP and silver determinations. Speciation diagrams based on the experimental concentrations of Cl^- and Ag^+ in aqueous media were created in MINTEQ (3.1).

2.7. Size distribution and dissolution of Ag-PVP NPs in specific wastewater constituents

The influence of PO_4^{3-}(9.5–47.5 mg/L), NH_4^+ (36–90 mg/L), and S^{2-} (0.32–32 mg/L) on the stability of Ag-PVP NPs with nominal size of 40 nm was studied in terms of size distribution and Ag dissolution, by using the NTA and sp-ICP-MS, respectively. Stock solutions of NH_4OH (3.5 g/L), K_2HPO_4 (1.74 g/L) and Na_2S (0.156 g/L) were prepared and adjusted to pH 7 ± 0.2 with 2% HNO_3. Aliquots from stocks were diluted with DI water to reach the experimental concentrations. Then, Ag-PVP NPs were spiked to achieve 100 μg/L. Solutions used in experiments containing S^{2-} were flushed with N_2 during 20 min to remove the dissolved oxygen, and provide anoxic conditions (Cervantes-Avilés et al., 2018). All the tubes were sonicated during 15 min, and left to stand 1 h until analysis. Speciation diagrams for experimental concentrations of S^{2-} and Ag^+ were created in MINTEQ.

3. Results and discussion

3.1. Calibration of the NTA and sp-ICP-MS

The concentration used in the calibration of NTA was 100 μg/L for both Ag-PVP NPs (40 nm) and Au (60 nm). According to the manufacturer, these concentrations correspond theoretically to 2.84×10^8 and 4.58×10^7 particles/mL, respectively. Measured concentrations via NTA for Ag and Au NPs were 3.93×10^8 and 6.80×10^7 particles/mL, respectively, which represent 1.4 and 1.5 times higher than theoretical particle concentrations (See supplementary information, Fig. S1). The overestimation in particle number has already been reported elsewhere for similar concentrations of Au NPs (Mehrabi et al., 2017), tracking up to 3 times more particles in DI water, and 2 times in landfill leachate. Our results indicate that the over counting of particles is also observed for Ag-PVP NPs, even though they are less stable than Au NPs and some dissolution may take place (Wimmer et al., 2018). The median sizes were 41 ± 5 nm for Ag-PVP and 58 ± 3 nm for Au (Fig. S1), in line with the nominal size. Hence, the overestimation in particle number of Ag-PVP and Au NPs did not affect the median size determination of either particle type. The size distribution for 90% of particles were between 26 and 67 nm for Ag and 40–75 nm for the Au particles. The amplitude of the size distribution also reflects that Au particles are more stable than Ag.

To calibrate the sp-ICP-MS, 100 ng/L of 60 nm Au NPs were used. During calibration, nanoparticle counts were clearly differentiated from the background ionic concentration (Fig. S2). A dwell time of 100 μs per point was suitable to distinguish the number of events (particles) from the ionic noise. The ability of microsecond sp-ICP-MS to improve the signal-to-noise ratio has been demonstrated for metal NPs (Montaño et al., 2014). The size distribution for the Au NPs 60 nm used as reference material was quite symmetric, and the median experimental size coincided with the nominal size (Fig. S2).

3.2. Ag-PVP NPs characterization

All nominal Ag-PVP NPs were negatively charged in DI water, with ZP between −19.7 and −23.8 mV (Fig. 1A), similar to other PVP-coated nano-Ag (Auvinen et al., 2017). The LSPR of Ag-PVP NPs clearly showed a size dependence (Fig. 1B). High linearity ($R^2 = 0.98$) was observed between nominal size of the Ag-PVP NPs and the corresponding LSPR (Fig. 1C), which moves towards the visible region as size increases. This indicates that Ag-PVP NPs smaller than 20 nm are more sensitive to ultraviolet radiation,

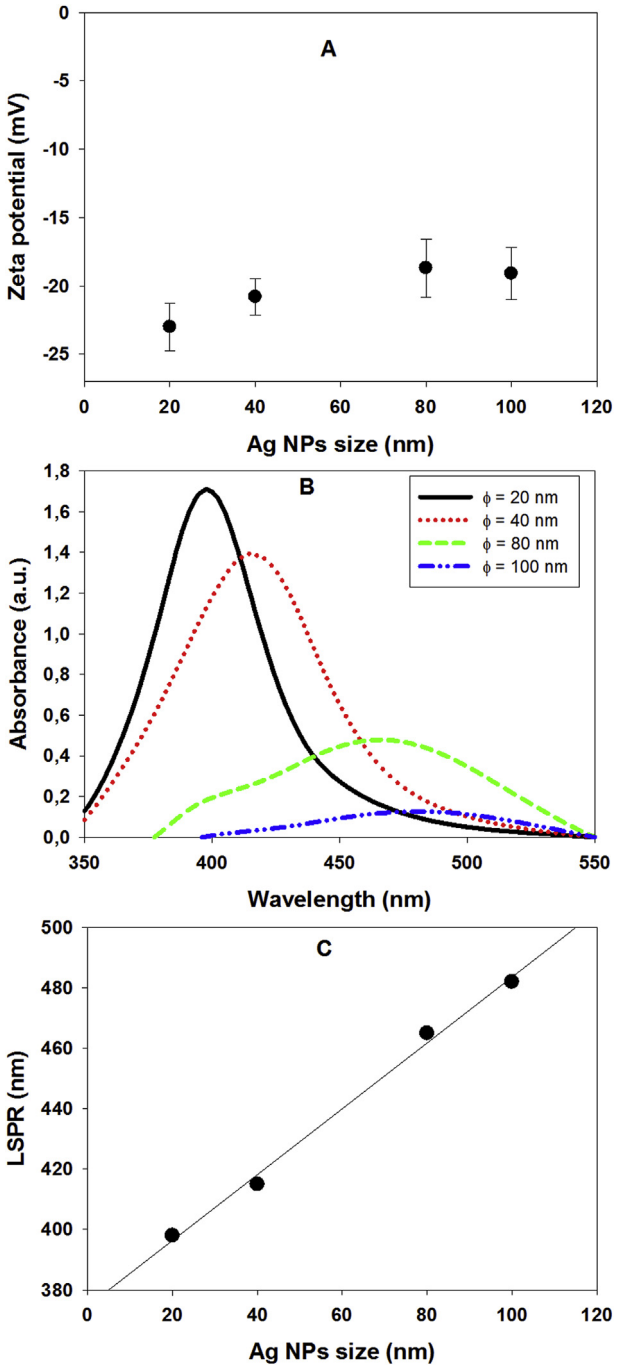

Fig. 1. Characterization of the Ag-PVP NPs with nominal sizes of 20, 40, 80 and 100 nm, in terms of (A) zeta potential, (B) ultraviolet–visible spectrum and (C) correlation between localized surface plasmon resonance (LSPR) and nominal size of Ag-PVP NPs.

while larger ones are optically sensitive in the visible region of the electromagnetic spectrum. For the nominal 20, 40, 80 and 100 nm Ag-PVP NPs, the median sizes, measured via NTA, were (all in nm) 28 ± 4, 41 ± 5, 75 ± 8 and 99 ± 4, and the sizes of 90% of the particles ranged from (all in nm) 18–55, 26–67, 45–119, and 76–138, respectively (Fig. S3). It was observed that for all nominal Ag-PVP NPs, the measured particle concentrations were also higher than the theoretical concentrations (Fig. S3). The over counting of particle concentration in the NTA can be also influenced by the particle size.

3.3. Stability of Ag-PVP NPs in synthetic wastewater over time

The response of LSPR of Ag particles with nominal sizes of 20, 40, 80 and 100 nm in SWW over time is observed in Fig. 2. According to LSPR, the persistence of Ag-PVP NPs in SWW was higher for those with nominal size of 80 and 100 nm, followed by 40 nm, and lowest for the 20 nm Ag-PVP NPs (Fig. 2), which was unexpected. The symbols of Ag-PVP NPs with 40 nm in Fig. 2 are behind those for 80 nm since both trends were very similar up to 150 min. Since the absorbance reflects only the persistence of original NPs, the missing fraction of the Ag-PVP NPs for all nominal sizes (1- A/A_0) can be attributed to both the partial dissolution of the Ag-PVP NPs and the precipitation of aggregates in SWW.

The aggregates formation was noted in the NTA measurements (Fig. 3). The size distribution for all nominal sizes was broader 5 h after spiking the Ag-PVP NPs, especially in the upper size range, which may contain aggregates (Fig. 3). In experiments with particles of nominal size of 80 and 100 nm, the amplitude in the size distribution for the 90% of the particles was 29–211 nm and 38–241 nm, respectively. The median size observed for 80 and 100 nm increased to 91 and 125, respectively, while that for 20 and 40 nm particles did not change substantially after 5 h (Fig. 3). Aggregate formation of Ag particles in SWW was also observed via the sp-ICP-MS measurements (Fig. 4). In experiments containing Ag particles with nominal size of 80 and 100 nm, aggregates up to 210 and 220 nm were detected respectively, which is in line with NTA measurements. For 40 nm Ag particles, the size distribution shifted to smaller sizes with particles of 30 nm as the most frequent size, although a few aggregates between 60 and 100 nm were observed. In the case of 20 nm Ag-PVP NPs in SWW, a few aggregates were also detected in the range of 60–120 nm. Compared to NTA, sp-ICP-MS showed a limitation for sizing nano-Ag below 18 nm. This has been already observed when nano-Ag are quantified and characterized in water or wastewater (Azimzada et al., 2017; Cervantes-Avilés et al., 2019; Hadioui et al., 2014; Lee et al., 2014). Hence, characterizing nano-Ag smaller than 20 nm by sp-ICP-MS is highly sensitive, even when using ion exchange resin column.

The percentage of dissolved Ag immediately after spiking the Ag-PVP NPs into SWW was between 4.06 and 10.96% for all particles at time 0 h (Table 3). After 5 h of exposure to SWW, the dissolved fraction of silver was between 8.7 and 19.27%. Dissolution of Ag from Ag-PVP NPs at PECs increased over time (0–5 h) for all nominal sizes (20, 40, 80 and 100 nm). However, the highest

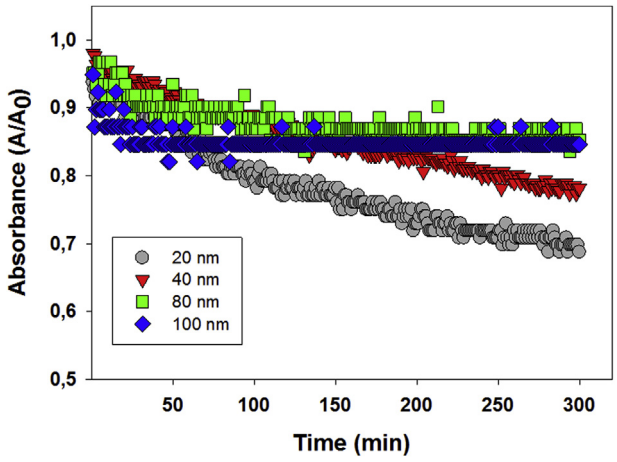

Fig. 2. Persistence of Ag-PVP NPs (20, 40, 80 and 100 nm) in synthetic wastewater (SWW) over 5 h as function of the relative absorbance of localized surface plasmon resonance (LSPR) at measured time (A) and at time zero (A_0).

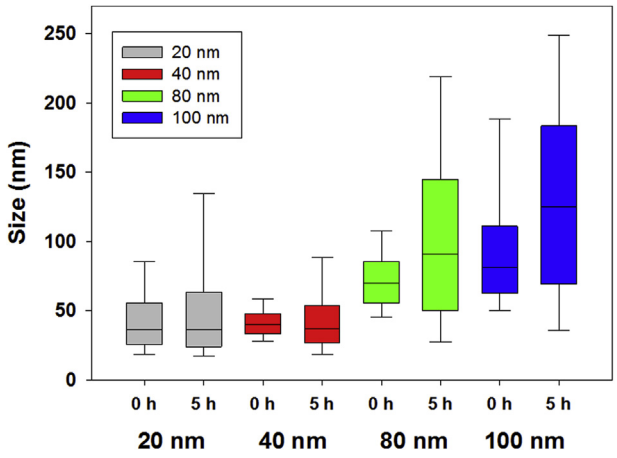

Fig. 3. Size distribution of Ag-PVP NPs (20, 40, 80 and 100 nm) by using nanoparticle tracking analysis (NTA) at different experimental time, immediately after spiking (0 h) and after 5 h of exposure to synthetic wastewater. The whisker width represents the sizes that occur 90% of the time, the inner box represents the values that occurs 50% of the time, and the central dash line represents the median value.

dissolution was observed for the smaller particles (20 nm). Hence, the decrease in the intensity of the LSPR for these NPs (Fig. 2) can be attributed mainly to the dissolution of particles. The dissolution of 40 nm Ag-PVP was also noticeable, 14.8% after 5 h of contact with SWW. Based on the sp-ICP-MS measurements, the median and the most frequent size of these particles became smaller (Table 3). The nominal particle size with less dissolved fraction at PECs were the 80 and 100 nm, which is in line with LSPR analysis (Fig. 2.), and indicates that these particles persisted more in suspension in SWW than smaller nominal sizes. As it is observed in Table 3, the median size of the 80 and 100 nm Ag-PVP NPs, increased after 5 h, which also agrees with the NTA measurements. The partial dissolution of Ag-PVP NPs is inferred by the particle concentration measured in the NTA, which decreased for all particle sizes at 5 h (Fig. S4). In the case of Ag-PVP NPs of 20 and 40 nm, the particles concentrations presented a clear peak of the most frequent size at 20 and 35 nm, respectively. For particles with nominal size of 80 and 100 nm, the particle concentration was distributed in a wide range from 25 to 250 nm, indicating both partial dissolution and aggregate formation. Increasing size, aggregate formation, and dissolution of Ag are a function of the wastewater composition. Since 40 nm Ag-PVP NPs exhibited both aggregation and dissolution, this nominal size was selected to study the effects of specific wastewater constituents (NOM, Cl^-, S^{2-}, PO_4^{3-} and NH_4^+) on the stability and dissolution of nAg.

3.4. *Influence of NOM and chloride on the size and surface charge of Ag-PVP NPs*

NOM and Cl^- are important components in wastewater and in many environmental water matrices. Based on the NTA measurements, the presence of NOM in aqueous media did not significantly affect the size distribution of nominal 40 nm Ag-PVP NPs (Fig. 5A). While the median size of the Ag-PVP NPs at different NOM concentrations remained close to the nominal size (40 nm), size distributions were in the range of 22–85 nm. Although nano-Ag are already functionalized, increasing NOM concentration resulted in a more negative ZP (Fig. 6A). NOM may become entangled with PVP in the surface of NPs (Yu et al., 2014). The observed stability of Ag-PVP NPs at PECs in combination with NOM (>5 μg/L) may favor their transport along the WWTP and other environmental water matrices, such as lentic, lotic, and coastal ecosystems.

In the case of Ag-PVP NPs exposed to Cl^-, their size distributions

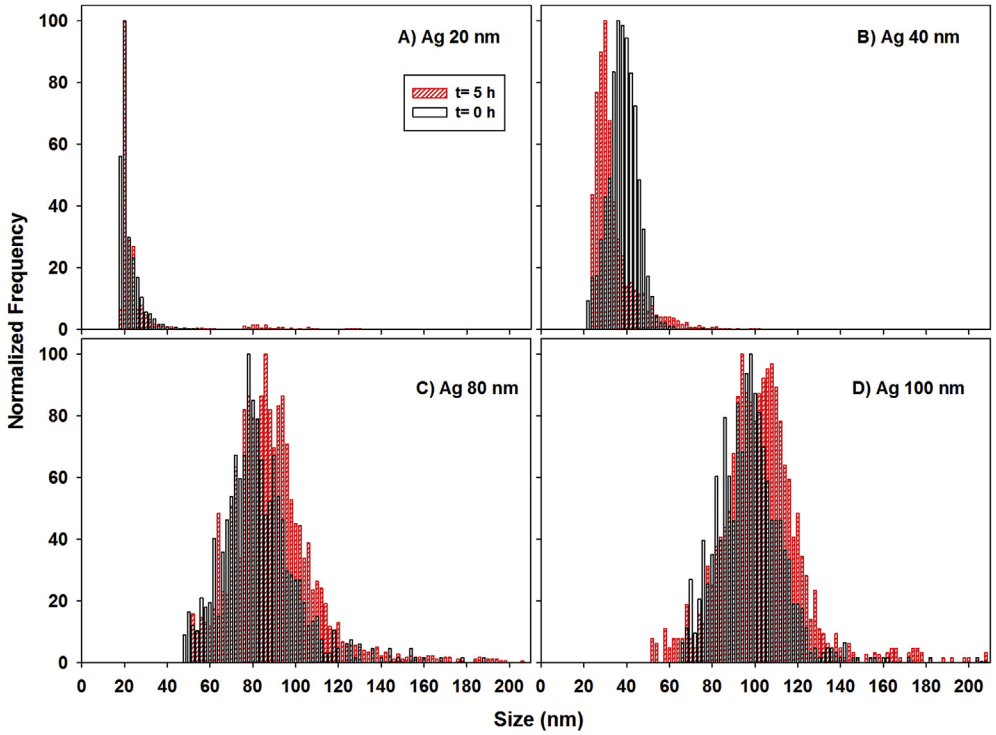

Fig. 4. Size distribution of Ag-PVP particles with nominal sizes of (A) 20 nm, (B) 40 nm, (C) 80 nm and (D) 100 nm, measured in synthetic wastewater (SWW) by single particle ICP-MS. Measurements correspond to time 0 h (black bars) immediately after spiked, and at 5 h of exposure to SWW (red lined bars). (For interpretation of the references to colour in this figure legend, the reader is referred to the Web version of this article.)

Table 3
Dissolution of Ag (%) from different nominal sizes of PVP- Ag nanoparticles (NPs) at time 0 h and 5 h of exposure to synthetic wastewater (SWW), and the median and most frequent size measured via single particle ICP-MS. Dissolved Ag percentages are the average of triplicates ± standard deviation.

	Dissolved Ag (%)		Median Size (nm)		Most Freq. Size (nm)	
Time of measurement (h)	0	5	0	5	0	5
Nominal size of NP						
PVP- Ag 20 nm	10.96 ± 0.80	19.27 ± 0.53	22 ± 2	26 ± 2	20 ± 1	20 ± 1
PVP- Ag 40 nm	6.84 ± 0.13	14.80 ± 0.38	38 ± 1	32 ± 4	36 ± 2	30 ± 4
PVP- Ag 80 nm	6.05 ± 0.43	9.24 ± 0.25	80 ± 2	90 ± 4	78 ± 2	86 ± 5
PVP- Ag 100 nm	4.06 ± 0.23	8.70 ± 0.37	95 ± 1	104 ± 6	98 ± 2	94 ± 8

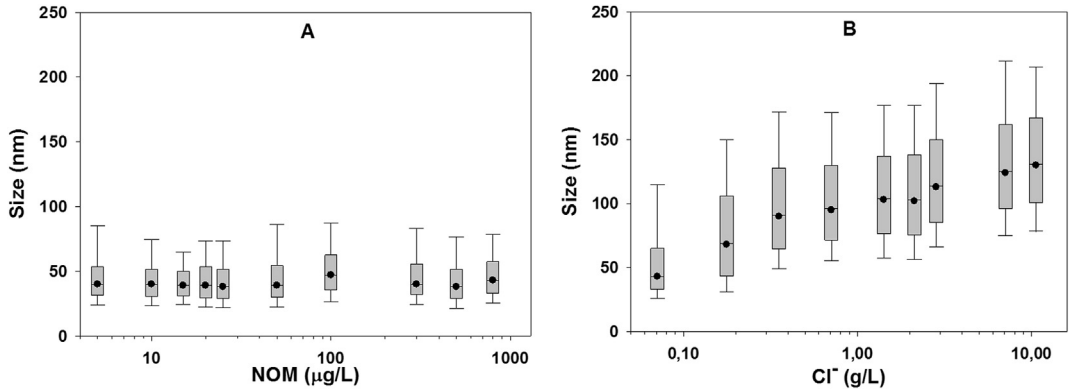

Fig. 5. Size distributions of Ag-PVP NPs (nominal size of 40 nm) measured via nanoparticle tracking analysis (NTA) in (A) natural organic matter (NOM) (5–800 µg/L), and (B) Cl^- (0.07–10.64 g/L). The whisker width represents the sizes of Ag-PVP NPs that occur 90% of the time, the inner box represents the values that occur 50% of the time, and the central dot represents the median size of the Ag-PVP NPs at the NOM and Cl^- concentration, respectively.

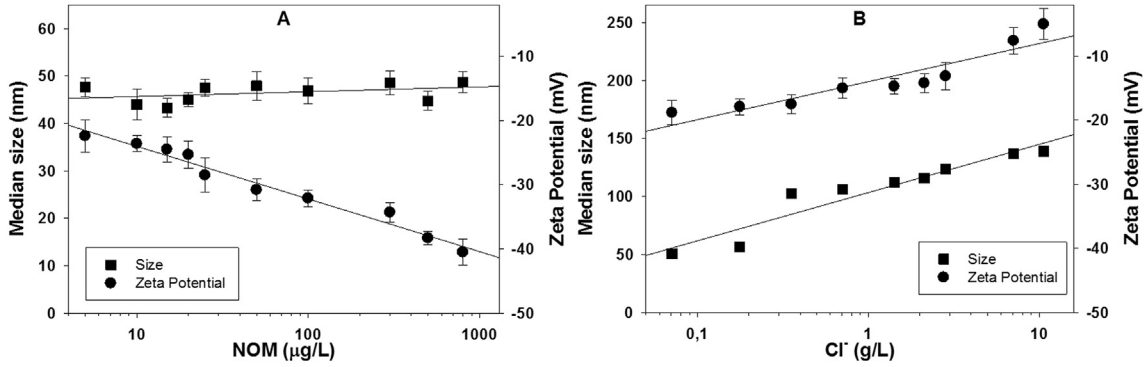

Fig. 6. Stability of the Ag-PVP NPs (40 nm) in terms of median size and zeta potential and after exposure (1 h) to (A) natural organic matter (NOM) and (B) Cl^-.

became much broader (Fig. 5B) than in the NOM experiments. The amplitude (5–95 percentiles) of the size distributions for all Cl^- tested were between 98 and 142 nm, with a maximum of up to 210 nm. In contrast to NOM experiments, the median size of the Ag-PVP particles increased by almost 3 times as the concentration of Cl^- increased from 0.07 to 10.64 g/L, while ZP tended to zero as the Cl^- concentration increased (Fig. 6B). The concentration of Ag particles decreased in the presence of Cl^-, except in the presence of 0.71, 1.42 and 2.13 g Cl^-/L (Fig. S5). This further suggests that as Ag was dissolving, it was rapidly precipitated around the core of the remaining NPs. The speciation diagrams created in MINTEQ (Fig. S6) may help to understand three key points of this experiment: (i) $AgCl_{(s)}$ is formed in the presence of ≤1.42 g Cl^-/L at low Ag^+ concentrations (≤140 µg/L); (ii) the precipitation of $AgCl_{(s)}$ in the presence of >2.13 g Cl^-/L is not thermodynamically favored; and (iii) the formation of $AgCl_x^{(x-1)-}$ species for all tested Cl^- concentrations can explain the partial dissolution of particles. Based on these points, one can infer the release of Ag^+, the equilibrium of the $AgCl_x^{(x-1)-}$ species and the formation of $AgCl_{(s)}$ as the shell growth of the particles, likely the deposition of an $AgCl/Ag_2O$ layer. Our results indicate that the formation of $AgCl_{(s)}$ could take place for molar ratios $Cl/Ag \geq 2100$ (at 0.07 g Cl^-/L) when nano-Ag are present at PECs. At higher nano-Ag concentration (mg/L), the formation of $AgCl_{(s)}$ was observed at lower Cl/Ag (≤535) (Levard et al., 2013b).

Dissolved Ag from Ag particles in the presence of NOM or Cl^- exhibited an opposite behavior (Fig. 7). Dissolution of Ag-PVP NPs at PECs decreased from 42.2 to 5.1% as NOM increased from 10 µg/L to 300 µg/L after 1 h of exposure (Fig. 7), probably because NOM

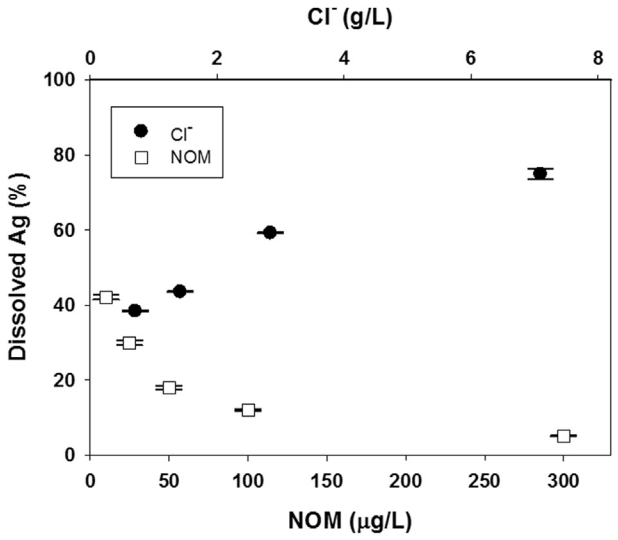

Fig. 7. Dissolved Ag from Ag-PVP 40 nm in presence of natural organic matter (NOM) and Chloride (Cl^-).

entangled with PVP inhibits the release of Ag^+ (Yu et al., 2014), or that NOM plays an important role in binding free Ag^+ (Wang et al., 2015). In either case, free Ag^+ would likely be at low concentrations in environments rich in NOM. In saline media, the dissolved Ag increased 38.4–74.9% in 1 h, as the concentration of Cl^- increased. Dissolved Ag from Ag-PVP NPs at PECs in saline media can rapidly form $AgCl_{(S)}$ and some of the soluble $AgCl_x^{(x-1)-}$ species. However, the overall dissolution in the environment can be higher since the residence time in many ecosystems is longer.

3.5. Effect of wastewater constituents (PO_4^{3-}, NH_4^+, and S^{2-}) on the stability of Ag-PVP NPs

In addition to organic matter and chloride, other wastewater constituents such as PO_4^{3-}, NH_4^+, and S^{2-} can play an important role in the aggregation and dissolution of Ag-PVP NPs. The size distribution of Ag-PVP NPs in aqueous media at low (9.5 mg/L) and high (47.5 mg/L) PO_4^{3-} did not reflect significant differences compared with that of Ag-PVP NPs in DI water (Fig. 8A). This is in contrast to other NPs, such as ZnO, CuO and Fe oxides, which interact significantly with PO_4^{3-} to form stable forms of phosphate (Daou et al., 2007; Herrmann et al., 2014; Ortelli et al., 2017). For Ag-PVP NPs exposed to a high phosphate concentration, the size distribution and particle concentration were similar to Ag-PVP NPs in the control (phosphate-free nanoPure water) (Fig. S7). In addition, the dissolved Ag was lower in the presence of a high concentration of phosphate (Fig. 9A), indicating that Ag-PVP NPs remain stable without significant dissolution at a high PO_4^{3-} concentration.

In the case of NH_4^+, the median size of Ag-PVP NPs did not change substantially at low (36 mg/L) NH_4^+ concentration but was noticeably increased at a high (90 mg/L) NH_4^+ level. The size distribution of Ag particles was broader at both low and high NH_4^+ concentrations relative to nanoPure water, with some particles larger than 200 nm (Fig. 8A). The particle concentration indicates that the number of particles between 50 and 200 nm increased as the ammonium concentration increased (Fig. S7), and there were fewer particles below 50 nm. Dissolution in 1 h was 26.3 and 48.5% of the initial load of nano-Ag for low and high ammonium concentration, respectively (Fig. 9A). Based on the speciation diagrams, the formation of $AgNH_3^+$ and $Ag(NH_3)_2^+$ may take place in these experimental conditions (Fig. S8).

The influence of sulfide on Ag-PVP NPs at PECs reflected a wider size distribution of Ag-PVP NPs with nominal size of 40 nm (Fig. 8B). The median size did not change significantly (55 nm in average) for all S^{2-} concentrations (Fig. 8B). This was also observed in the particle concentration plots, where the peaks were between 50 and 60 nm for all S^{2-} concentrations (Fig. S7). Besides, the particle concentration increased as the concentration of S^{2-} in the media increased (Fig. S7). If we consider that the concentration of Ag^+ decreased as the sulfide present in media increased (Fig. 9B), and that the speciation diagrams performed in MINTEQ predicted that more than 99% of the Ag^+ forms stable $Ag_2S_{(s)}$ at these experimental S^{2-} concentrations (Fig. S9), then, the increased size of the Ag particles at PECs is attributed to the formation of an $Ag_2S_{(s)}$ shell. This experiment confirms that $Ag_2S_{(s)}$ formation on nano-Ag at PECs is very likely in wastewater with >0.32 mg/L of sulfide. The coarsening of Ag particles with $Ag_2S_{(s)}$ has been already reported in previous experiments, which were performed at concentrations much higher than the PECs, namely 50 mg/L (Kaegi et al., 2013) and ≥97 mg/L (Levard et al., 2011).

4. Conclusions

In this work, we applied NTA, sp-ICP-MS and LSPR to study the stability and dissolution of Ag-PVP NPs with nominal sizes of 20, 40, 80 and 100 nm at PECs in wastewater and its important

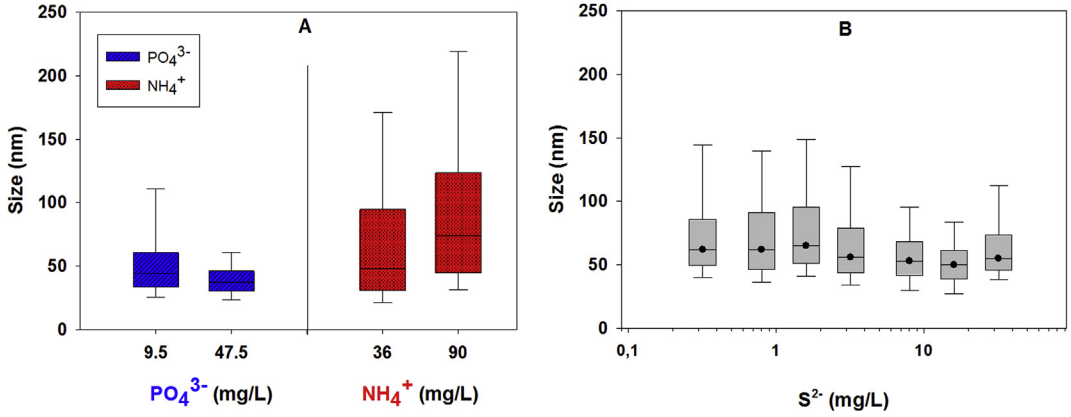

Fig. 8. Size distributions of suspensions of 100 µg/L Ag-PVP NPs (nominal size of 40 nm) measured via nanoparticle tracking analysis (NTA) in (A) PO_4^{3-} (9.5 and 47.5 mg/L), NH_4^+ (36 and 90 mg/L) and (B) S^{2-} (0.32–32.1 mg/L). The whisker width represents the sizes that occur 90% of the time, the inner box represents the values that occurs 50% of the time, and the central dash line represents the median value.

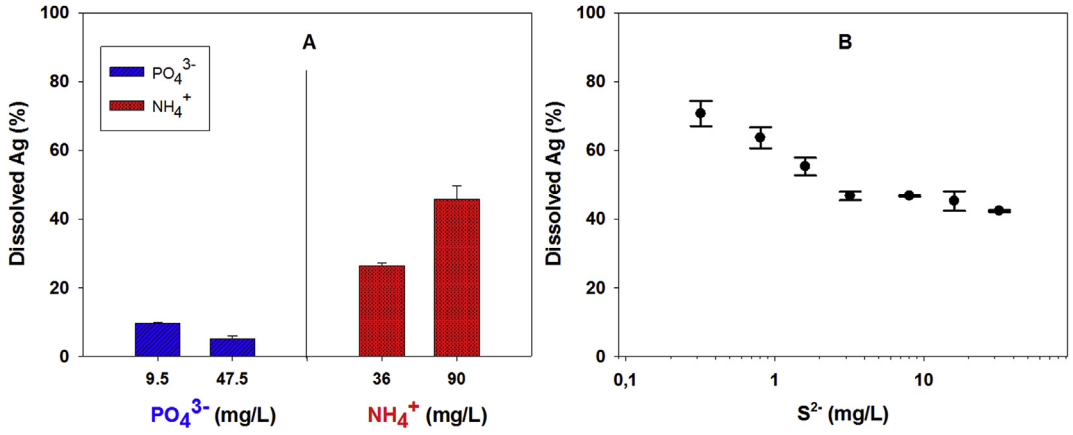

Fig. 9. Concentration of Ag^{+} in the presence of (A) PO_4^{3-} (9.5 and 47.5 mg/L), NH_4^{+} (36 and 90 mg/L) and (B) S^{2-} (0.32–32.1 mg/L).

constituents such as NOM, Cl^{-}, PO_4^{3-}, NH_4^{+} and S^{2-}. Although dissolution of nano-Ag at PECs in SWW was observed for all nominal sizes, smaller nanoparticles were dissolved more after 5 h of exposure, 14.8% and 19.27% of initial load of 40 and 20 nm nano-Ag, respectively. The LSPR analysis was in line with the dissolution levels measured, indicating that Ag particles with nominal size of 80 and 100 nm were more persistent than those with nominal size of 20 and 40 nm. NTA and sp-ICP-MS resulted in very similar size distributions of nano-Ag at PECs in SWW. Both techniques detected aggregate formation in SWW after 5 h, especially for 80 and 100 nm nano-Ag, which ranged in NTA from 29 to 211 nm and 38–241 nm, respectively; and via sp-ICP-MS from 48 to 210 nm and 50–220 nm, respectively. With regards to the effect of wastewater constituents on the stability and dissolution of Ag-PVP NPs at PECs, even at low concentrations of NOM (>5 μg/L) and PO_4^{3-} (9.5 mg/L) the dissolution of Ag decreased and their presence served to stabilize the Ag-PVP NPs. The presence of NH_4^{+} led the dissolution of 26.3% and 48.5% of the initial load of Ag-PVP NPs, for low and high ammonium concentration in water, mainly forming soluble $AgNH_3^{+}$ and $Ag(NH_3)_2^{+}$. However, Cl^{-} and S^{2-} drive the dissolution and precipitation of newly formed solids, either in the shell of the original NPs or as separate particles. Our experiments indicated that $AgCl_{(s)}$ may form preferentially at molar ratios $Cl/Ag \geq 2100$ at PECs, and that $Ag_2S_{(s)}$ formation can be a strong pattern in wastewater with >0.32 mg/L of sulfide for nano-Ag at PECS. In all cases including the SWW, full dissolution of the Ag particles was not observed even at PECs, within the timeframe of these experiments (0–5 h). Hence, a fraction of the original particles, possibly with a stabilizing shell, could pass through the WWTP onto the aquatic environment. Additional insights are gained when performing these experiments at PECs, such as the interactions with the main wastewater constituents. The combined use of NTA and sp-ICP-MS can serve to better understand the size distributions and particles concentrations over time, as well as the physicochemical transformation of a dynamic nanoscale system.

Declaration of competing interest

The authors declare that they have no known competing financial interests or personal relationships that could have appeared to influence the work reported in this paper.

Acknowledgments

This work was supported by the National Science Foundation (NSF) and the U.S. Environmental Protection Agency under cooperative agreement number NSF-EF0830117. Arturo A. Keller also appreciates Agilent Technologies for their Agilent Thought Leader Award. Pabel Cervantes-Aviles thanks CONACYT for his postdoctoral fellowship (330129). Any opinions, findings, conclusions, or recommendations expressed in this material are those of the authors do not necessarily reflect the views of the funding agencies.

Appendix A. Supplementary data

Supplementary data to this article can be found online at https://doi.org/10.1016/j.watres.2019.115072.

References

APHA, 2005. Standard methods for the examination of water and wastewater. Stand. Methods 541 https://doi.org/ISBN_9780875532356.

Auvinen, H., Gagnon, V., Rousseau, D.P.L., Du Laing, G., 2017. Fate of metallic engineered nanomaterials in constructed wetlands: prospection and future research perspectives. Rev. Environ. Sci. Biotechnol. 16, 207–222. https://doi.org/10.1007/s11157-017-9427-0.

Azimzada, A., Tufenkji, N., Wilkinson, K.J., 2017. Transformations of silver nanoparticles in wastewater effluents: links to Ag bioavailability. Environ. Sci. Nano 4, 1339–1349. https://doi.org/10.1039/c7en00093f.

Bitragunta, S.P., Palani, S.G., Gopala, A., Sarkar, S.K., Kandukuri, V.R., 2017. Detection of TiO2 nanoparticles in municipal sewage treatment plant and their characterization using single particle ICP-MS. Bull. Environ. Contam. Toxicol. 98, 595–600. https://doi.org/10.1007/s00128-017-2031-8.

Blaser, S.A., Scheringer, M., MacLeod, M., Hungerbühler, K., 2008. Estimation of cumulative aquatic exposure and risk due to silver: contribution of nano-functionalized plastics and textiles. Sci. Total Environ. 390, 396–409. https://doi.org/10.1016/j.scitotenv.2007.10.010.

Brar, S.K., Verma, M., 2011. Measurement of nanoparticles by light-scattering techniques. TrAC Trends Anal. Chem. (Reference Ed.) 30, 4–17. https://doi.org/10.1016/j.trac.2010.08.008.

Brunetti, G., Donner, E., Laera, G., Sekine, R., Scheckel, K.G., Khaksar, M., Vasilev, K., De Mastro, G., Lombi, E., 2015. Fate of zinc and silver engineered nanoparticles in sewerage networks. Water Res. 77, 72–84. https://doi.org/10.1016/j.watres.2015.03.003.

Cao, C., Huang, J., Yan, C., Liu, J., Hu, Q., Guan, W., 2018. Shifts of system performance and microbial community structure in a constructed wetland after exposing silver nanoparticles. Chemosphere 199, e34. https://doi.org/10.1016/j.chemosphere.2018.02.031.

Carr, B., Wright, M., 2013. Nanoparticle Tracking Analysis A Review of Applications and Usage 2010 – 2012, vol. 1. NanoSight Ltd, p. 188.

Cascio, C., Geiss, O., Franchini, F., Ojea-Jimenez, I., Rossi, F., Gilliland, D., Calzolai, L., 2015. Detection, quantification and derivation of number size distribution of silver nanoparticles in antimicrobial consumer products. J. Anal. At. Spectrom. 30, 1255–1265. https://doi.org/10.1039/c4ja00410h.

Cervantes-Avilés, P., Brito, E.M.S., Duran, R., Martínez, A.B., Cuevas-Rodríguez, G., 2016. Effect of ZnO nanoparticles in the oxygen uptake during aerobic wastewater treatment. J. Nanoparticle Res. 18. https://doi.org/10.1007/s11051-016-3481-3.

Cervantes-Avilés, P., Díaz Barriga-Castro, E., Palma-Tirado, L., Cuevas-Rodríguez, G., 2017. Interactions and effects of metal oxide nanoparticles on microorganisms

involved in biological wastewater treatment. Microsc. Res. Tech. 80, 1103–1112. https://doi.org/10.1002/jemt.22907.
Cervantes-Avilés, P., Huang, Y., Keller, A.A., 2019. Incidence and persistence of silver nanoparticles throughout the wastewater treatment process. Water Res. 156, 188–198. https://doi.org/10.1016/j.watres.2019.03.031.
Cervantes-Avilés, P., Ida, J., Toda, T., Cuevas-rodríguez, G., 2018. Effects and Fate of TiO 2 Nanoparticles in the Anaerobic Treatment of Wastewater and Waste Sludge, vol. 222, pp. 227–233. https://doi.org/10.1016/j.jenvman.2018.05.074.
Daou, T.J., Begin-Colin, S., Pourroy, G., Legaré, P., Thomas, F., Bernhardt, P., Grenèche, J.M., Derory, A., 2007. Phosphate adsorption properties of magnetite-based nanoparticles. Chem. Mater. 19, 4494–4505. https://doi.org/10.1021/cm071046v.
Degueldre, C., Favarger, P.Y., 2003. Colloid analysis by single particle inductively coupled plasma-mass spectroscopy: a feasibility study. Colloids Surfaces A Physicochem. Eng. Asp. 217, 137–142. https://doi.org/10.1016/S0927-7757(02)00568-X.
Delay, M., Dolt, T., Woellhaf, A., Sembritzki, R., Frimmel, F.H., 2011. Interactions and stability of silver nanoparticles in the aqueous phase: influence of natural organic matter (NOM) and ionic strength. J. Chromatogr. A 1218, 4206–4212. https://doi.org/10.1016/j.chroma.2011.02.074.
Domingos, R.F., Baalousha, M. a, Ju-nam, Y., Reid, M.M., Tufenkji, N., Lead, J.R., Leppard, G.G., Wilkinson, K.J., 2009. Characterizing manufactured nanoparticles in the Environment : multimethod determination of particle sizes characterizing manufactured nanoparticles in the Environment : multimethod determination of particle sizes. Environ. Sci. Technol. 7277–7284. https://doi.org/10.1021/es900249m.
Donovan, A.R., Adams, C.D., Ma, Y., Stephan, C., Eichholz, T., Shi, H., 2016. Single particle ICP-MS characterization of titanium dioxide, silver, and gold nanoparticles during drinking water treatment. Chemosphere 144, 148–153. https://doi.org/10.1016/j.chemosphere.2015.07.081.
Doolette, C.L., McLaughlin, M.J., Kirby, J.K., Batstone, D.J., Harris, H.H., Ge, H., Cornelis, G., 2013. Transformation of PVP coated silver nanoparticles in a simulated wastewater treatment process and the effect on microbial communities. Chem. Cent. J. 7, 1. https://doi.org/10.1186/1752-153X-7-46.
Hadioui, M., Peyrot, C., Wilkinson, K.J., 2014. Improvements to single particle ICPMS by the online coupling of ion exchange resins. Anal. Chem. 86, 4668–4674. https://doi.org/10.1021/ac5004932.
Herrmann, R., García-García, F.J., Reller, A., 2014. Rapid degradation of zinc oxide nanoparticles by phosphate ions. Beilstein J. Nanotechnol. 5, 2007–2015. https://doi.org/10.3762/bjnano.5.209.
Impellitteri, C.A., Tolaymat, T.M., Scheckel, K.G., 2009. The speciation of silver nanoparticles in antimicrobial fabric before and after exposure to a hypochlorite/detergent solution. J. Environ. Qual. 38, 1528. https://doi.org/10.2134/jeq2008.0390.
Ivask, A., Kurvet, I., Kasemets, K., Blinova, I., Aruoja, V., Suppi, S., Vija, H., Kakïnen, A., Titma, T., Heinlaan, M., Visnapuu, M., Koller, D., Kisand, V., Kahru, A., 2014. Size-dependent toxicity of silver nanoparticles to bacteria, yeast, algae, crustaceans and mammalian cells in vitro. PLoS One 9. https://doi.org/10.1371/journal.pone.0102108.
Jin, Z., Zhang, X., Li, J., Yang, F., Kong, D., Wei, R., Huang, K., Zhou, B., 2017. Impact of wastewater treatment plant effluent on an urban river. J. Freshw. Ecol. 32, 697–710. https://doi.org/10.1080/02705060.2017.1394917.
Kaegi, R., Voegelin, A., Ort, C., Sinnet, B., Thalmann, B., Krismer, J., Hagendorfer, H., Elumelu, M., Mueller, E., 2013. Fate and transformation of silver nanoparticles in urban wastewater systems. Water Res. 47, 3866–3877. https://doi.org/10.1016/j.watres.2012.11.060.
Keller, A.A., Huang, Y., Nelson, J., 2018. Detection of nanoparticles in edible plant tissues exposed to nano-copper using single-particle ICP-MS. J. Nanoparticle Res. 20. https://doi.org/10.1007/s11051-018-4192-8.
Keller, A.A., Lazareva, A., 2013. Predicted releases of engineered nanomaterials: from global to regional to local. Environ. Sci. Technol. Lett. 1, 65–70. https://doi.org/10.1021/ez400106t.
Korenstein, R., Horev-Azaria, L., Roesslein, M., Manø, S., Wiemann, M., Haase, A., Vennemann, A., Dybowska, A., Anguissola, S., Hannell, C., Cooke, L., Wick, P., Capracotta, S., Hole, P., Magdolenova, Z., Contal, S., Riediker, M., Staunton, K.C., Sillence, K., Sauvain, J.-J., Prina-Mello, A., Suarez, G., Luch, A., Maguire, C.M., Gutleb, A.C., Dusinska, M., 2013. Interlaboratory comparison of size measurements on nanoparticles using nanoparticle tracking analysis (NTA). J. Nanoparticle Res. 15. https://doi.org/10.1007/s11051-013-2101-8.
Laborda, F., Bolea, E., Jiménez-Lamana, J., 2014. Single particle inductively coupled plasma mass spectrometry: a powerful tool for nanoanalysis. Anal. Chem. 86, 2270–2278. https://doi.org/10.1021/ac402980q.
Lazareva, A., Keller, A.A., 2014. Estimating potential life cycle releases of engineered nanomaterials from wastewater treatment plants. ACS Sustain. Chem. Eng. 2, 1656–1665. https://doi.org/10.1021/sc500121w.
Lead, J.R., Batley, G.E., Alvarez, P.J.J., Croteau, M.N., Handy, R.D., McLaughlin, M.J., Judy, J.D., Schirmer, K., 2018. Nanomaterials in the environment: behavior, fate, bioavailability, and effects—an updated review. Environ. Toxicol. Chem. 37, 2029–2063. https://doi.org/10.1002/etc.4147.
Lee, S., Bi, X., Reed, R.B., Ranville, J.F., Herckes, P., Westerhoff, P., 2014. Nanoparticle size detection limits by single particle ICP-MS for 40 elements. Environ. Sci. Technol. 48, 10291–10300. https://doi.org/10.1021/es502422v.
Levard, C., Hotze, E.M., Colman, B.P., Dale, A.L., Truong, L., Yang, X.Y., Bone, A.J., Brown, G.E., Tanguay, R.L., Di Giulio, R.T., Bernhardt, E.S., Meyer, J.N., Wiesner, M.R., Lowry, G.V., 2013a. Sulfidation of silver nanoparticles: natural antidote to their toxicity. Environ. Sci. Technol. 47, 13440–13448. https://doi.org/10.1021/es403527n.
Levard, C., Hotze, E.M., Lowry, G.V., Brown, G.E., 2012. Environmental transformations of silver nanoparticles: impact on stability and toxicity. Environ. Sci. Technol. 46, 6900–6914. https://doi.org/10.1021/es2037405.
Levard, C., Mitra, S., Yang, T., Jew, A.D., Badireddy, A.R., Lowry, G.V., Brown, G.E., 2013b. Effect of chloride on the dissolution rate of silver nanoparticles and toxicity to E. coli. Environ. Sci. Technol. 47, 5738–5745. https://doi.org/10.1021/es400396f.
Levard, C., Reinsch, B.C., Michel, F.M., Oumahi, C., Lowry, G.V., Brown, G.E., 2011. Sulfidation processes of PVP-coated silver nanoparticles in aqueous solution: impact on dissolution rate. Environ. Sci. Technol. 45, 5260–5266. https://doi.org/10.1021/es2007758.
Li, L., Hartmann, G., Döblinger, M., Schuster, M., 2013. Quantification of nanoscale silver particles removal and release from municipal wastewater treatment plants in Germany. Environ. Sci. Technol. 47, 7317–7323. https://doi.org/10.1021/es3041658.
Li, Y., Zhao, J., Shang, E., Xia, X., Niu, J., Crittenden, J., 2018. Effects of chloride ions on dissolution, ROS generation, and toxicity of silver nanoparticles under UV irradiation. Environ. Sci. Technol. 52, 4842–4849. https://doi.org/10.1021/acs.est.7b04547.
Liu, T., Liu, S., Zheng, M., Chen, Q., Ni, J., 2016. Performance assessment of full-scale wastewater treatment plants based on seasonal variability of microbial communities via high-throughput sequencing. PLoS One 11. https://doi.org/10.1371/journal.pone.0152998.
Louie, S.M., Tilton, R.D., Lowry, G.V., 2016. Critical review: impacts of macromolecular coatings on critical physicochemical processes controlling environmental fate of nanomaterials. Environ. Sci. Nano 3, 283–310. https://doi.org/10.1039/c5en00104h.
Lowry, G.V., Espinasse, B.P., Badireddy, A.R., Richardson, C.J., Reinsch, B.C., Bryant, L.D., Bone, A.J., Deonarine, A., Chae, S., Therezien, M., Colman, B.P., Hsu-Kim, H., Bernhardt, E.S., Matson, C.W., Wiesner, M.R., 2012. Long-term transformation and fate of manufactured Ag nanoparticles in a simulated large scale freshwater emergent wetland. Environ. Sci. Technol. 46, 7027–7036. https://doi.org/10.1021/es204608d.
Lusk, M.G., Toor, G.S., Yang, Y.Y., Mechtensimer, S., De, M., Obreza, T.A., 2017. A review of the fate and transport of nitrogen, phosphorus, pathogens, and trace organic chemicals in septic systems. Crit. Rev. Environ. Sci. Technol. 47, 455–541. https://doi.org/10.1080/10643389.2017.1327787.
Ma, R., Levard, C., Judy, J.D., Unrine, J.M., Martin, B., Jefferson, B., Lowry, G.V., Durenkamp, M., 2013. Fate of Zinc Oxide and Silver Nanoparticles in a Pilot Waste Water Treatment Plant and in Processed Biosolids Fate of Zinc Oxide and Silver Nanoparticles in a Pilot Waste Water Treatment Plant and in Processed Biosolids.
Maurer-Jones, M.A., Gunsolus, I.L., Murphy, C.J., Haynes, C.L., 2013. Toxicity of engineered nanoparticles in the environment. Anal. Chem. 85, 3036–3049. https://doi.org/10.1021/ac303636s.
McGillicuddy, E., Murray, I., Kavanagh, S., Morrison, L., Fogarty, A., Cormican, M., Dockery, P., Prendergast, M., Rowan, N., Morris, D., 2017. Silver nanoparticles in the environment: sources, detection and ecotoxicology. Sci. Total Environ. 575, 231–246. https://doi.org/10.1016/j.scitotenv.2016.10.041.
Mehrabi, K., Nowack, B., Arroyo Rojas Dasilva, Y., Mitrano, D.M., 2017. Improvements in nanoparticle tracking analysis to measure particle aggregation and mass distribution: a case study on engineered nanomaterial stability in incineration landfill leachates. Environ. Sci. Technol. 51, 5611–5621. https://doi.org/10.1021/acs.est.7b00597.
Metcalf, E., Eddy, M., 2014. Wastewater Engineering: Treatment and Resource Recovery. Mic Graw-Hill, USA, pp. 1530–1533.
Mitrano, D.M., Lesher, E.K., Bednar, A., Monserud, J., Higgins, C.P., Ranville, J.F., 2012. Detecting nanoparticulate silver using single-particle inductively coupled plasma-mass spectrometry. Environ. Toxicol. Chem. 31, 115–121. https://doi.org/10.1002/etc.719.
Montaño, M.D., Badiei, H.R., Bazargan, S., Ranville, J.F., 2014. Improvements in the detection and characterization of engineered nanoparticles using spICP-MS with microsecond dwell times. Environ. Sci. Nano 1, 338–346. https://doi.org/10.1039/c4en00058g.
Ortelli, S., Badetti, E., Blosi, M., Costa, A.L., Brunelli, A., Hristozov, D., Bonetto, A., Marcomini, A., 2017. Colloidal characterization of CuO nanoparticles in biological and environmental media. Environ. Sci. Nano 4, 1264–1272. https://doi.org/10.1039/c6en00601a.
Roesslein, M., 2018. Particle Tracking Analysis Measuring the Size and Concentration of Nanoparticles Using Particle Tracking Analysis (PTA) 1–16.
Sekine, R., Brunetti, G., Donner, E., Khaksar, M., Vasilev, K., Jämting, A.K., Scheckel, K.G., Kappen, P., Zhang, H., Lombi, E., 2015. Speciation and lability of Ag-, AgCl-, and Ag2S-nanoparticles in soil determined by X-ray absorption spectroscopy and diffusive gradients in thin films. Environ. Sci. Technol. 49, 897–905. https://doi.org/10.1021/es504229h.
Sun, T.Y., Bornhöft, N.A., Hungerbühler, K., Nowack, B., 2016. Dynamic probabilistic modeling of environmental emissions of engineered nanomaterials. Environ. Sci. Technol. 50, 4701–4711. https://doi.org/10.1021/acs.est.5b05828.
van Loosdrecht, M.C., Nielsen, P.H., Lopez-Vazquez, C.M., Brdjanovic, D., 2016. Experimental Methods in Wastewater Treatment. https://doi.org/10.1017/CBO9781107415324.004.
Wang, H., Adeleye, A.S., Huang, Y., Li, F., Keller, A.A., 2015. Heteroaggregation of nanoparticles with biocolloids and geocolloids. Adv. Colloid Interface Sci. 226,

24–36. https://doi.org/10.1016/j.cis.2015.07.002.
Westerhoff, P., Atkinson, A., Fortner, J., Wong, M.S., Zimmerman, J., Gardea-Torresdey, J., Ranville, J., Herckes, P., 2018. Low risk posed by engineered and incidental nanoparticles in drinking water. Nat. Nanotechnol. 13, 661–669. https://doi.org/10.1038/s41565-018-0217-9.
Westerhoff, P., Lee, S., Yang, Y., Gordon, G.W., Hristovski, K., Halden, R.U., Herckes, P., 2015. Characterization, recovery opportunities, and valuation of metals in municipal sludges from U.S. Wastewater treatment plants nationwide. Environ. Sci. Technol. 49, 9479–9488. https://doi.org/10.1021/es505329q.
Wimmer, A., Kalinnik, A., Schuster, M., 2018. New insights into the formation of silver-based nanoparticles under natural and semi-natural conditions. Water Res. 141, 227–234. https://doi.org/10.1016/j.watres.2018.05.015.
Yu, S., Yin, Y., Zhou, X., Dong, L., Liu, J., 2016. Transformation kinetics of silver nanoparticles and silver ions in aquatic environments revealed by double stable isotope labeling. Environ. Sci. Nano 3, 883–893. https://doi.org/10.1039/c6en00104a.
Yu, S.J., Yin, Y.G., Chao, J.B., Shen, M.H., Liu, J.F., 2014. Highly dynamic PVP-coated silver nanoparticles in aquatic environments: chemical and morphology change induced by oxidation of Ag^0 and reduction of Ag^+. Environ. Sci. Technol. 48, 403–411. https://doi.org/10.1021/es404334a.
Zhang, C., Hu, Z., Deng, B., 2016. Silver nanoparticles in aquatic environments: physiochemical behavior and antimicrobial mechanisms. Water Res. 88, 403–427. https://doi.org/10.1016/j.watres.2015.10.025.
Zhang, W., Xiao, B., Fang, T., 2018. Chemical transformation of silver nanoparticles in aquatic environments: mechanism, morphology and toxicity. Chemosphere 191, 324–334. https://doi.org/10.1016/j.chemosphere.2017.10.016.